RESEARCH ARTICLE | APRIL 01 2025

Theoretical study of the excited states of NeH and of their non-adiabatic couplings: A preliminary for the modeling of the dissociative recombination of NeH^+

R. Hassaine ✉; D. Talbi ; R. P. Brady ; J. Zs. Mezei ; J. Tennyson ; I. F. Schneider

J. Chem. Phys. 162, 134302 (2025)
https://doi.org/10.1063/5.0261152

The Journal of Chemical Physics ARTICLE pubs.aip.org/aip/jcp

Theoretical study of the excited states of NeH and of their non-adiabatic couplings: A preliminary for the modeling of the dissociative recombination of NeH^+

Cite as: J. Chem. Phys. 162, 134302 (2025); doi: 10.1063/5.0261152
Submitted: 29 January 2025 • Accepted: 16 March 2025 •
Published Online: 1 April 2025

R. Hassaine,[1,a)] D. Talbi,[2,b)] R. P. Brady,[3] J. Zs. Mezei,[1,4] J. Tennyson,[1,3] and I. F. Schneider[1,5]

AFFILIATIONS

[1] LOMC CNRS-UMR6294, Université le Havre Normandie, F-76058 Le Havre, France
[2] LUPM CNRS-UMR5299, Université de Montpellier, F-34095 Montpellier, France
[3] Department of Physics and Astronomy, University College London, WC1E 6BT London, United Kingdom
[4] HUN-REN Institute for Nuclear Research (ATOMKI), H-4001 Debrecen, Hungary
[5] LAC CNRS-UMR9188, Université Paris-Saclay, F-91405 Orsay, France

[a)] **Author to whom correspondence should be addressed:** riyad.hassaine@univ-lehavre.fr
[b)] **Electronic mail:** dahbia.talbi@umontpellier.fr

ABSTRACT

Potential energy curves and matrix elements of radial non-adiabatic couplings of the $^2\Sigma^+$ and $^2\Pi$ states of the NeH molecule are calculated using the electronic structure package MOLPRO, in view of the study of the reactive collisions between low-energy electrons and NeH^+.

I. INTRODUCTION

Neon is envisaged as a coolant in the divertor of the International Thermonuclear Experimental Reactor (ITER),[1–4] since it can absorb energy via its excitation and ionization through reactions with rapid electrons. Dielectronic recombination of the formed ions, followed by the electronic relaxation process,

$$Ne^+ + e^- \rightarrow Ne^{**} \rightarrow Ne + h\nu, \tag{1}$$

allows safe dissipation of heat along the walls through radiation. On and near the surface of the reactor, collisions between neon atoms with vibrationally excited $H_2{}^+$ can produce NeH^+,

$$Ne + H_2^+(v_i^+ > 1) \rightarrow NeH^+ + H, \tag{2}$$

the reaction for ground state ions being endothermic by 0.54 eV.[3] The presence of NeH^+ in the edge plasma implies the need for quantifying the reactivity of this ion. This quantification can be achieved from the calculation of the cross sections and rate coefficients, which characterize the efficiency of collisions between NeH^+ and other species present in the plasma. Among them, the collisions with electrons, resulting in dissociative recombination (DR)[4] and vibrational transitions (VTs),

$$NeH^+ + e^- \rightarrow NeH^*, NeH^{**} \rightarrow \begin{cases} Ne + H & (DR), \\ NeH^{+*} + e^- & (VT), \end{cases} \tag{3}$$

are particularly important.

Cross sections for the DR of NeH^+ were already measured at the storage ASTRID ring, with results reported in 2005.[3] Theoretical evaluations of the cross sections have also been performed for collision energies ranging between 5 and 22 eV,[4] and they agree with the experimental ones between 6 and 10 eV.[3] So far, theoretical results have not been available for the physically important electron collision energies below 5 eV, where experiment[3] measures significant cross sections of about 10^{-18} cm^2.

The low energy DR of the hydride cations relying on the elements preceding and following neon in the Periodic Table—helium and argon, respectively—is well understood and quantified. Helium

and argon were the subject of detailed investigations[5,6] focusing on their abundances in the interstellar media, and both are present in the edge plasma.

HeH^+, one of the oldest molecules in the Universe, was observed in 2016 in the nebula NGC 7027.[7] It is the simplest molecular prototype that recombines with electrons exclusively through the indirect pathway, proceeding via electron capture into Rydberg states, without having a diabatic dissociative neutral state that crosses the cation.[8,9] The initial state-selective measurements performed on the Cryogenic Storage Ring[10] have shown a dramatic decrease in the DR rate coefficients at very low collision energies, which can cause higher abundances in cold interstellar environments. The most recent calculations of Čurik *et al.*[11,12] using energy-dependent rovibrational frame transformation combined with Multichannel Quantum Defect Theory (MQDT) have confirmed the experimental observations.

As for ArH^+, it was detected more than one decade ago in the Crab Nebula.[13] Prior to its discovery, Mitchell *et al.*[14] working in the ASTRID storage ring had estimated the anisotropic rate coefficient below 2 eV lower than 10^{-9} cm^3 s^{-1}. The molecular structure of ArH was addressed,[15] and it was found that the asymptotic limit of the lowest diabatic electronic state of this molecule is 1.822 eV above the ground vibrational level, which implies—if restricted exclusively to Rydberg–valence coupling—no recombination below this energy and, consequently, a negligible rate coefficient.[16] However, Kálosi *et al.*[17] measured low but non-negligible DR rates into the ground state of ArH, claiming the mechanism of non-adiabatic coupling between the ionization continuum and the ground electronic state. This scenario is supported by theoretical considerations in the same study, as well as computations in progress by Larson and Orel.[17]

Unlike HeH^+[7] and ArH^+,[13] NeH^+ remains undetected in these media. Recent work by Sil *et al.*[6] suggests that NeH^+ could be formed in nova ejecta via the reaction

$$Ne + HeH^+ \rightarrow NeH^+ + He,$$

with a rate coefficient of ~10^{-9} cm^3 s^{-1}. This pathway appears more likely than the alternative reaction proposed by Theis *et al.*,[18]

$$Ne^+ + H_2 \rightarrow NeH^+ + H,$$

which is considered unfavorable. The formation of NeH^+ is expected to be heavily dependent on the abundance of HeH^+, which is more prevalent due to the significant presence of helium and atomic hydrogen in the environment. However, NeH^+ production is constrained by the low cosmological abundance of neon[5] and the underabundance of molecular hydrogen. Another potential explanation for the non-detection of NeH^+ may lie in its DR behavior. A high DR rate coefficient at interstellar medium relevant temperatures could significantly reduce its steady-state concentration, making detection more challenging.

Below 5 eV, the lack of theoretical data for the cross sections can be initially addressed by producing the *ab initio* adiabatic potential energy curves (PECs) of NeH corresponding to the bound Rydberg states energetically open for dissociation (below $v_i^+ = 0$ of the ion's ground state), similarly to Refs. 19–23, and non-adiabatic couplings responsible for the transitions among the different Born–Oppenheimer adiabatic states. Here, we consider both the relevant NeH PECs and compute the matrix elements, which give the radial non-adiabatic couplings (NACs) between all the explored states of the neutral. In the current study, we focus on these two aspects, while the dynamical calculations will be considered in a further study, relying on the current molecular structure data results.

TABLE I. H atom Rydberg basis set.

Type	Exponent	Coefficient
s	0.006 685	1.0
s	0.002 670	1.0
p	0.024 684	1.0
p	0.007 169	1.0
p	0.002 867	1.0
d	0.003 600	1.0

The organization of this paper is as follows: In Sec. II, the computational steps are presented. Section III contains the results—PECs, spectroscopic data, NACs—and we provide the concluding remarks in Sec. IV.

II. COMPUTATIONAL DETAILS

The potential energy curve calculations for NeH and NeH^+ in its ground state were carried out using the MOLPRO quantum chemistry program suite[24] at the Multi-Configurational Self-Consistent Field (MCSCF)—Multi-Reference Configuration Interaction (MRCI) level of theory with a complete active space (CAS) of 8,3,3,0 orbitals in the C_{2v} point-group symmetry. The CAS corresponds to the complete valence active space extended to include the $n = 2$ and $n = 3$ orbitals of hydrogen. We started with the augmented correlation-consistent polarized valence triple zeta (aug-cc-pVTZ) basis sets implemented in MOLPRO, and we have extended the hydrogenic part of the basis by two *s*, three *p*, and one *d* diffuse atomic orbitals (AOs) with exponents from Ref. 21, which are given in Table I.

In this way, the chosen basis set provides a more accurate description of the states correlating with the $n = 2$ and $n = 3$ hydrogen dissociation limits.

For the neutral molecule, the MCSCF wave functions were optimized by state-averaging the five lowest $^2\Sigma^+$ states (5 A_1 states in the C_{2v} symmetry of the calculation) and the two lowest $^2\Pi$ states ($^2B_2/^2B_1$ states in the C_{2v} symmetry of the calculation). To summarize, the ground state of NeH^+, $X\ ^1\Sigma^+$, and the lowest seven states of NeH, respectively, $X\ ^2\Sigma^+$, $A\ ^2\Sigma^+$, $B\ ^2\Pi$, $C\ ^2\Sigma^+$, $4\ ^2\Sigma^+$, $2\ ^2\Pi$, and $5\ ^2\Sigma^+$ have been calculated.

The NACs between the states of the neutral were calculated using the following expressions:[9,25]

$$A_{ij}(R) = \left\langle \psi_i^\Gamma(\{\vec{r}\}, R) \middle| \frac{\partial}{\partial R} \middle| \psi_j^\Gamma(\{\vec{r}\}, R) \right\rangle_{\{\vec{r}\}}, \tag{4}$$

$$B_{ij}(R) = \left\langle \psi_i^\Gamma(\{\vec{r}\}, R) \middle| \frac{\partial^2}{\partial R^2} \middle| \psi_j^\Gamma(\{\vec{r}\}, R) \right\rangle_{\{\vec{r}\}} = \frac{\partial A_{ij}(R)}{\partial R} - A_{ij}^2(R). \tag{5}$$

Here, Γ stands for the symmetry of the molecular state, *i* and *j* denote different electronic states belonging to the same symmetry,

and we focus exclusively on couplings that satisfy $i < j$. R is the internuclear distance, and $\{\vec{r}\}$ denotes the complete set of electronic coordinates linked to the electrons of the neutral. In order to calculate the NACs using Eqs. (4) and (5), one has to integrate over the electronic coordinates. This is achieved numerically using the MOLPRO derivative coupling (DDR) procedure for $A(R)$ and by using the central finite difference scheme for the derivative to obtain $B(R)$. The spectroscopic description of the target, including the 15 vibrational levels of the ground state of NeH^+, were obtained by using the Numerov–Cooley method[26,27] to solve the nuclear-motion Schrödinger equation.

III. RESULTS AND DISCUSSIONS

Figure 1 displays the *ab initio* PECs of the ground electronic state of NeH^+ $\left(^1\Sigma^+\right)$ (blue curve), the repulsive ground electronic state of NeH, and the mono-excited Rydberg states of NeH for both symmetries $^2\Sigma^+$ and $^2\Pi$, up to the Ne + H($n = 3$) dissociation limit (black curves). The dissociative ground state of the neutral X $^2\Sigma^+$ correlates with the Ne + H($1s$) atomic limit, where Ne stands for the $^1S_0$ ground state of atomic neon. The excited states correlating with the Ne + H($n = 2$) limits from bottom to top are A $^2\Sigma^+$ – B $^2\Pi$ – C $^2\Sigma^+$, and the states tending to the Ne + H($n = 3$) are 4 $^2\Sigma^+$ – 2 $^2\Pi$ – 5 $^2\Sigma^+$. Our results compare well with those from Theodorakopoulos *et al.*[20] (red curves).

Figure 2 shows the NACs $A(R)$ corresponding to Eq. (4) between the molecular states having $^2\Sigma^+$ (solid curves) and $^2\Pi$ (dashed curves) symmetry, up to the Ne + H($n = 3$) dissociation limit. The couplings involving the highest excited state 5 $^2\Sigma^+$ are not shown as their magnitudes are negligible (approximately 10^{-8} a_0^{-1}). One can notice that the couplings of the $^2\Sigma^+$ states are the more important ones, while the coupling involving the two $^2\Pi$ states is about one order of magnitude smaller. Similarly to PECs,

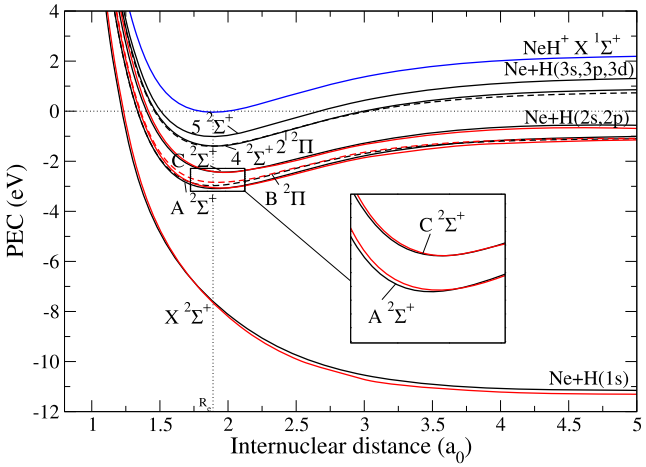

FIG. 1. *Ab initio* PECs of the ground electronic state of NeH^+ and of the lowest—ground and Rydberg—electronic states of NeH. The black solid lines stand for the neutral with $^2\Sigma^+$ symmetry, the black dashed lines represent the neutral with $^2\Pi$ symmetry, and the blue solid line corresponds to the ion's ground state X $^1\Sigma^+$. Our results are compared with the calculations of Theodorakopoulos *et al.*[20] (red lines).

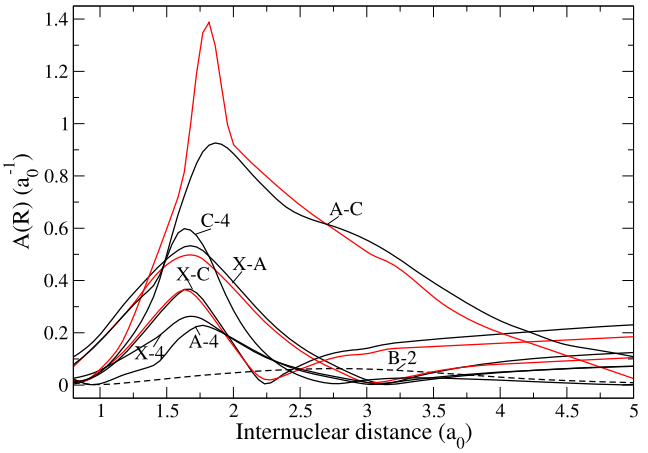

FIG. 2. Radial non-adiabatic couplings $A(R)$. The color code is the same as for Fig. 1.

we have compared our NACs (in black) with those calculated by Theodorakopoulos *et al.*[20] presented in red. One can conclude that the current results are consistent with the previous ones. The sharp peak of the A–C coupling is due to the strong interaction between these two electronic states.

Figure 3 contains all the NACs $A(R)$ given by Eq. (4) (already shown in Fig. 2), in comparison with $B(R)$ given by Eq. (5). One can see that the most significant $B(R)$ NAC is the A–C one, followed by C–4, X–A, X–C, X–4, A–4, and B–2, which predicts the importance of the Rydberg correlating with the Ne + H($n = 3$) limit for the internuclear dynamics.

To fully characterize the molecular system, we have calculated the major spectroscopic data of the molecular target and for the neutral system. They are shown in Tables II, III, IV, and V, where our results are compared with previous theoretical results,[3,4,22,23,30–38] experimental results,[28,29,33] and data from the NIST Chemistry WebBook.[39]

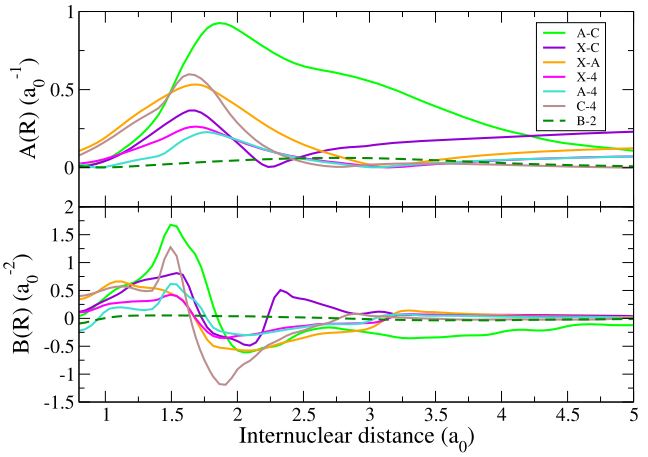

FIG. 3. First-derivative radial non-adiabatic couplings $A(R)$ and second-derivative radial non-adiabatic couplings $B(R)$, between the states of NeH.

TABLE II. Equilibrium separation (R_e), absolute minimum energy [$E(R_e)$], and well-depth (D_e) for NeH^+ ($X\,^1\Sigma^+$) PECs: comparison with the theoretical "T" as well as experimental "exp." data from the literature. Data from the present work are labeled as "PW". ε_0 represents the percentage difference between the calculations and the experimental measurements for D_e. All other: Atomic orbitals calculated with SCF.

Source	Level of theory	Basis set	R_e (a_0)	$E(R_e)$ (Hartree)	D_e(eV)	ε_0 (%)
Exp[28,29]			1.873 10	...	2.275 11	
PW	MRCI[a]	See Sec. II	1.891 99	−128.896 45	2.268 88	0.27
T[30]	CCSD(T)	CBS	1.873 28	−128.953 63	2.291 97	0.74
T[30]	MRCI + Q	AV6Z	1.873 28	−128.948 51	2.296 13	0.92
T[31]	...	...	1.872 91	...	2.178 69	4.43
T[32]	MRCI	aug-AO	1.875 55	...	2.287 51	0.54
T[4]	CI	TZP	1.893 50	...	2.320 00	1.93
T[23]	SCF	cc-pVTZ	1.862 70	−128.881 05	2.370 00	4.00
T[3]	CI	aug-AO	1.870 83	...	2.148 31	5.90
T[33]	MRCISD[b]	...	1.873 10	...	2.296 15	0.92
T[22]	MRDCI	aug-AO	1.894 83	−128.978 70	2.290 00	0.65
T[34]	MRCI[b]	aug-AO	1.876 50	...	2.310 00	1.51
T[35]	CEPA[c]	AO	1.881 98	−128.349 03	2.275 98	0.04
T[36]	SCF	STO	1.850 04	−128.624 20	2.100 00	8.34
T[36]	CI	STO	1.868 94	−128.681 80	2.270 00	0.23
T[37]	MRDCI	aug-AO	1.867 00	...	2.430 00	6.37
T[38]	MRCI	cc-pV5Z	1.873 00	...	2.299 00	1.03

[a]Atomic orbitals calculated with MCSCF.
[b]Atomic orbitals calculated with SCF-CASSCF.
[c]Atomic orbitals calculated with SCEP.

Table II refers to the molecular ion and shows values for its equilibrium geometry, the potential energy at equilibrium, and its dissociation energy. We compare our calculated parameters with other theoretical results[3,4,22,23,30–38] and evaluate the relative differences of the dissociation energy in contrast to the experimental measurements.[28,29] Our results agree well with existing experimental and other theoretical results, typically within 2%, except for a few studies[3,23,31,36,37] that employed lower levels of theory.

TABLE III. Calculated vibrational energy levels $E_{v_i}^+$ (eV) for NeH^+ ($X^1\Sigma^+$) with respect to $E_0 = -128.889\,98$ Hartree, and comparison with the experimental values from Refs. 28 and 33. The relative differences between our results and the experimental data are given by ε_0 (%).

v_i^+	This work	Exp.	ε_0 (%)
1	0.335 24	0.331 97	0.98
2	0.640 55	0.635 93	0.72
3	0.919 20	0.912 67	0.71
4	1.169 81	1.161 38	0.72
5	1.392 13	1.382 33	0.70
6	1.585 60	1.574 72	0.69
7	1.749 69	1.737 99	0.67
8	1.883 30	1.871 32	0.64
9	1.986 43	1.973 91	0.63
10	2.058 81	2.046 29	0.61
11	2.102 62	2.089 83	0.61
12	2.123 84	2.110 51	0.63
13	2.123 84	2.117 31	0.31
14	2.123 84	2.118 95	0.23

TABLE IV. Comparison of our computed NeH^+ ($X\,^1\Sigma^+$) and NeH Rydberg state dissociation limits relative to Ne + H(n = 1) (eV) with previous theoretical results[22,23] and data from NIST Chemistry WebBook.[39] The relative differences between our results and the NIST data are given by ε_0 (%).

Level	This work	Petsalakis *et al.*[22]	Lo *et al.*[23]	NIST	ε_0 (%)
n = 2	10.205 09	10.217 88	10.202 09	10.198 80	0.062
n = 3	12.093 83	12.108 53	12.092 01	12.087 50	0.052
H IP	13.554 81	13.568 15	13.579 45	13.598 40	0.322

In Table III, we list all the 15 vibrational levels of the cation calculated using the Numerov–Cooley method and compare them with experimental observations.[28,33] The relative differences obtained are below 1%, which confirms the accuracy of our structure calculations.

Table IV gives the dissociation limits of the electronic states of NeH^+ ($X\,^1\Sigma^+$) and of the NeH Rydberg states relative to Ne + H(n = 1), in comparison with previously computed limits[22,23] and with data from the NIST Chemistry WebBook.[39]

Finally, Table V contains the excitation energies of NeH^+ and of NeH electronic states relative to the A $^2\Sigma^+$ state of NeH for all electronic states above the same A $^2\Sigma^+$ state, calculated at the equilibrium distance of the ion.

The corresponding energy differences $\Delta E(R_e)$ are compared with the previous calculations.[22,23] One may notice that, except

TABLE V. Energy differences $\Delta E(R_e)$ (eV) at the equilibrium distance R_e of the NeH^+ ground electronic state, between several states and the NeH lowest excited electronic state ($A\,^2\Sigma^+$). The results are compared with the previous theoretically obtained data.[22,23]

State	This work	Petsalakis *et al.*[22]	Lo *et al.*[23]
$B\,^2\Pi$	0.120 45	0.223 65	0.174 99
$C\,^2\Sigma^+$	0.671 90	0.704 51	0.647 47
$2\,^2\Pi$	1.696 63	1.632 68	1.662 43
$4\,^2\Sigma^+$	1.705 31	1.722 14	1.627 43
$5\,^2\Sigma^+$	2.082 65	1.990 53	...
$X\,^1\Sigma^+$	3.054 59	3.142 35	3.079 87

for the B state, where a significant gap occurs, the agreement is satisfactory.

Our computational framework does not take into account the Rydberg states of NeH built on the excited states of the NeH^+ ion. For several molecular species, these "intruder" states play a visible role in the spectroscopy of the neutral and in its dynamics. However, this happens only when the lowest excited states of the ion are close to the ground one, which is not the case for NeH^+.[32] Therefore, we assert that our results are accurate, since not being affected by the core-excited Rydberg state effects.

IV. CONCLUSIONS

The potential energy curves for the ground state $^1\Sigma^+$ of the NeH^+ ion and for the lowest five $^2\Sigma^+$ states and two $^2\Pi$ states of the NeH molecule have been computed with high precision using the MOLPRO quantum chemistry suite at the MCSCF-MRCI level of theory, employing an extended complete active space (CAS) and augmented basis sets optimized for dissociation up to Ne + H ($n = 3$). The results show good agreement with previous experimental and theoretical studies, particularly with the work of Theodorakopoulos *et al.*,[20] Petsalakis *et al.*,[22] and Lo *et al.*[23] for some of these states. While the non-adiabatic couplings $A(R)$ between the states (A–C, X–A, X–C) up to Ne + H($n = 2$) had already been addressed by Theodorakopoulos *et al.*,[20] our calculations went beyond this producing further, namely both the couplings $A(R)$ and $B(R)$ between states dissociating up to the limit Ne + H($n = 3$)—X–4, A–4, C–4, X–5, A–5, C–5 for the $^2\Sigma^+$ symmetry and B–2 for the $^2\Pi$ symmetry. These couplings are essential for the calculation of cross sections and rate coefficients in low-energy collisions between electrons and NeH^+.[40,41] Work on this is currently in progress.

SUPPLEMENTARY MATERIAL

The supplementary material provides tabulated data for the potential energy curves shown in Fig. 1 and the non-adiabatic coupling terms $A(R)$ and $B(R)$ presented in Fig. 3.

ACKNOWLEDGMENTS

The authors acknowledge the support provided by the Fédération de Recherche Fusion par Confinement Magnétique (CNRS and CEA), La Région Normandie, LabEx EMC3 through projects PTOLEMEE, COMUE Normandie Université, and the Institute for Energy, Propulsion and Environment (FR-IEPE). J.Zs.M. acknowledges the financial support from the National Research, Development and Innovation Fund of Hungary, under the FK 19 funding schemes with Project No. FK 132989. This work was granted access to the HPC/AI resources of (CINES/IDRIS/TGCC) under the allocation 2023–2024 (Grant No. AD010805116R2) made by GENCI.

AUTHOR DECLARATIONS

Conflict of Interest

The authors have no conflicts to disclose.

Author Contributions

R. Hassaine: Conceptualization (equal); Data curation (equal); Formal analysis (lead); Investigation (equal); Methodology (equal); Writing – original draft (lead); Writing – review & editing (lead). **D. Talbi**: Conceptualization (equal); Data curation (equal); Methodology (lead); Supervision (lead); Validation (lead); Writing – original draft (equal); Writing – review & editing (equal). **R. P. Brady**: Methodology (equal); Software (lead); Writing – original draft (supporting); Writing – review & editing (equal). **J. Zs. Mezei**: Conceptualization (equal); Data curation (equal); Formal analysis (equal); Funding acquisition (lead); Investigation (equal); Methodology (equal); Project administration (equal); Supervision (equal); Validation (equal); Writing – original draft (lead); Writing – review & editing (lead). **J. Tennyson**: Conceptualization (lead); Formal analysis (equal); Investigation (lead); Methodology (equal); Supervision (lead); Validation (equal); Writing – original draft (supporting); Writing – review & editing (lead). **I. F. Schneider**: Conceptualization (lead); Formal analysis (supporting); Funding acquisition (lead); Investigation (equal); Methodology (supporting); Project administration (lead); Supervision (lead); Validation (lead); Writing – original draft (supporting); Writing – review & editing (lead).

DATA AVAILABILITY

The data that support the findings of this study are available within the article and its supplementary material.

REFERENCES

[1] D. Zajfman, J. B. A. Mitchell, B. R. Rowe, and D. Schwalm, *Dissociative Recombination, Theory, Experiment and Applications III* (World Scientific, 1996).
[2] J. B. A. Mitchell, *Atomic and Plasma-Material Interaction Data for Fusion* (IAEA, Vienna, 2001), Vol. 9, p. 97.
[3] J. B. A. Mitchell, O. Novotny, G. Angelova, J. L. LeGarrec, C. Rebrion-Rowe, A. Svendsen, L. H. Andersen, A. I. Florescu-Mitchell, and A. E. Orel, J. Phys. B: At., Mol. Opt. Phys. **38**, 693 (2005).
[4] V. Ngassam, A. I. Florescu-Mitchell, and A. E. Orel, Phys. Rev. A **77**, 042706 (2008).
[5] G. J. Schwarz, Astrophys. J. **577**, 940 (2002).
[6] M. Sil, A. Das, R. Das, R. Pandey, A. Faure, H. Wiesemeyer, P. Hily-Blant, F. Lique, and P. Caselli, Astron. Astrophys. **692**, A264 (2024).

[7]R. Güsten, H. Wiesemeyer, D. Neufeld, K. M. Menten, U. U. Graf, K. Jacobs, B. Klein, O. Ricken, C. Risacher, and J. Stutzki, Nature **568**, 357 (2019).
[8]B. K. Sarpal, J. Tennyson, and L. A. Morgan, J. Phys. B: At. Mol. Opt. Phys **27**, 5943 (1994).
[9]S. L. Guberman, Phys. Rev. A **49**, R4277 (1994).
[10]O. Novotný, P. Wilhelm, D. Paul, Á. Kálosi, S. Saurabh, A. Becker, K. Blaum, S. George, J. Göck, M. Grieser *et al.*, Science **365**, 676 (2019).
[11]R. Čurík, D. Hvizdoš, and C. H. Greene, Phys. Rev. Lett. **124**, 043401 (2020).
[12]D. Hvizdoš, C. H. Greene, and R. Čurík, Phys. Rev. A **101**, 012709 (2020).
[13]M. J. Barlow, B. M. Swinyard, P. J. Owen, J. Cernicharo, H. L. Gomez, R. J. Ivison, O. Krause, T. L. Lim, M. Matsuura, S. Miller *et al.*, Science **342**, 1343 (2013).
[14]J. B. A. Mitchell, O. Novotny, J. L. LeGarrec, A. Florescu-Mitchell, C. Rebrion-Rowe, A. V. Stolyarov, M. S. Child, A. Svendsen, M. A. E. Ghazaly, and L. H. Andersen, J. Phys. B: At., Mol. Opt. Phys. **38**, L175 (2005).
[15]A. Abdoulanziz, F. Colboc, D. A. Little, Y. Moulane, J. Z. Mezei, E. Roueff, J. Tennyson, I. F. Schneider, and V. Laporta, Mon. Not. R. Astron. Soc. **479**, 2415 (2018).
[16]E. Djuissi, A. Bultel, J. Tennyson, I. F. Schneider, and V. Laporta, Plasma Sources Sci. Technol. **31**, 114012 (2022).
[17]Á. Kálosi, M. Grieser, L. W. Isberner, H. Kreckel, Å. Larson, D. A. Neufeld, A. E. Orel, D. Paul, D. W. Savin, S. Schippers *et al.*, Phys. Rev. A **110**, 022816 (2024).
[18]R. A. Theis, W. J. Morgan, and R. C. Fortenberry, Mon. Not. R. Astron. Soc. **446**, 195 (2015).
[19]G. Theodorakopoulos, S. C. Farantos, R. J. Buenker, and S. D. Peyerimhoff, J. Phys. B: At. Mol. Phys **17**, 1453 (1984).
[20]G. Theodorakopoulos, R. J. Buenker, and I. D. Petsalakis, J. Phys. B: At. Mol. Phys **20**, 5335 (1987).
[21]S. Baer, D. G. Fleming, J. J. Sloan, D. J. Arseneau, M. Kolbuszewski, J. Wright, M. Senba, J. J. Pan, and R. Snooks, J. Chem. Phys. **101**, 1202 (1994).
[22]I. D. Petsalakis, G. Theodorakopoulos, Y. Li, G. Hirsch, R. J. Buenker, and M. S. Child, J. Chem. Phys. **108**, 7607 (1998).
[23]J. M. H. Lo, M. Klobukowski, D. Bielińska-Waż, G. H. F. Diercksen, and E. W. S. Schreiner, J. Phys. B: At. Mol. Phys. **38**, 1143 (2005).
[24]H. J. Werner, P. J. Knowles, G. Knizia, F. R. Manby, M. Schütz, P. Celani, W. Györffy, D. Kats, T. Korona, R. Lindh *et al.*, "Molpro, version 2022.1, a package of *ab initio* programs," WIREs Comput. Mol. Sci. (2022), https://www.molpro.net.
[25]R. P. Brady, C. Drury, S. N. Yurchenko, and J. Tennyson, J. Chem. Theory Comput. **20**, 2127 (2024).
[26]B. V. Noumerov, Mon. Not. R. Astron. Soc. **84**, 592 (1924).
[27]B. Numerov, Astron. Nachr. **230**, 359 (1927).
[28]R. S. Ram, P. F. Bernath, and J. W. Brault, J. Mol. Spectrosc. **113**, 451 (1985).
[29]H. Hotop, T. E. Roth, M. W. Ruf, and A. J. Yencha, Theor. Chim. Acta **100**, 36 (1998).
[30]M. J. Montes de Oca-Estevez and R. Prosmiti, Front. Chem. **9**, 664693 (2021).
[31]J. A. Coxon and P. G. Hajigeorgiou, J. Mol. Spectrosc. **330**, 63 (2016).
[32]B. Gerivani, A. Shayesteh, and A. Maghari, Comput. Theor. Chem. **1070**, 82 (2015).
[33]S. Civiš, J. Šebera, V. Špirko, J. Fišer, W. P. Kraemer, and K. Kawaguchi, J. Mol. Struct. **695**, 5 (2004).
[34]W. P. Kraemer, M. Juřek, and V. Špirko, "Vibration-rotational spectroscopy and molecular dynamics," in *Advances in Quantum Chemical and Spectroscopical Studies of Molecular Structures and Dynamics*, edited by D. Papoušek (World Scientific, 1997), p. 516.
[35]P. Rosmus and E. A. Reinsch, Z. Naturforsch. A **35**, 1066 (1980).
[36]V. Bondybey, P. K. Pearson, H. F. Schaefer III, and F. Henry, J. Chem. Phys. **57**, 1123 (1972).
[37]Y. Wan, P. Leiberman, R. Buenker, S. D. Loch, D. R. Schultz, and P. C. Stancil, Astrophys. J. **881**, 3 (2019).
[38]P. G. Yan and J. F. Babb, Astrophys. J. **961**, 43 (2024).
[39]P. Linstorm, *NIST Chemistry Webbook*, NIST Standard Reference Database Number 69 (National Institute of Standards and Technology, 1998).
[40]A. Giusti, J. Phys. B: At. Mol. Phys **13**, 3867 (1980).
[41]J. Z. Mezei, K. Chakrabarti, M. D. Epée Epée, O. Motapon, C. H. Yuen, M. A. Ayouz, N. Douguet, S. Fonseca dos Santos, V. Kokoouline, and I. F. Schneider, ACS Earth Space Chem. **3**, 2376 (2019).